Tidal Predictions Using a Frequency-Domain Model

JUANG Wen-Jye[1], TSAY Ting-Kuei[2], LIN Ming-Chung[3]

[1] Mathematic Modeling Division, Institute of Harbor and Marine Technology

[2] Department of Civil Engineering, National Taiwan University

[3] Department of Naval Architecture and Ocean Engineering,

National Taiwan University

Abstract

A 2-D frequency-domain linear shallow-water wave model including the Coriolis effects is applied to compute the harmonic constants of main tidal constituents around the coast of Taiwan. Good agreements between the computed results and of field data have been obtained for semidiurnal constituents (Lin, et al., 2000b). The computed harmonic constants obtained from the model thus are applied to predict tides incorporating with the IOS package. Good agreements are observed at stations where semidiurnal tides are predominant, or during the time spans of spring tide. Discrepancies are found at the stations where diurnal constituents are predominant, especially during the periods of neap tide. The new approach to compute spatial distribution of harmonic constants provides a mean for tidal predictions at gauged and ungauged sites.

1. Introduction

Taiwan situates right along the rim of the Asia Continental Shelf. With the predominant topographical effects of the shelf, abnormally large tidal range appears at the central western coast while very small ones are observed both at northern and southern ends of Taiwan. During the past several decades, the peculiar tidal characteristics have attracted great attentions from many researchers. Thorough investigations, however, were scarcely found. By using a frequency-domain model developed originally by Tsay (1991), semidiurnal constituents result in co-oscillation resonance due to the topographical effects has been demonstrated by Lin, et al. (2000a), recently. A partially standing wave appeared on the shelf has been verified (Lin, et al, 2000b) to illustrate the tidal characteristics appearing along the west coast of Taiwan. The frequency-domain model demonstrates its excellent capabilities to capture the physical characteristics of tides and thus will be further applied to tidal prediction.

In this paper, the frequency-domain model will be reviewed first. Verifications the computational results for specific constituents, such as M_2 and K_1, will be presented next. Using the computational harmonic constants obtained from the frequency-domain model, tidal prediction incorporated with the package of IOS (the Institute of Ocean Sciences) will be demonstrated and discussed subsequently. Conclusions are summarized in the last section.

2. A frequency-domain tidal model

Basing on the linear shallow-water wave equations with the Coriolis effects, the two-dimensional model equation (Tsay, 1991) is suitable for monochromatic tides over varying topography :

$$\nabla \bullet (PG\nabla\varsigma) + k^2 PG\varsigma = 0 , \qquad (1)$$

where $\nabla = (\partial/\partial x, \partial/\partial y)$ denotes the space gradient operator on the horizontal right-hand Cartesian coordinate (x, y) ; P and G are phase and group velocity, respectively; $\varsigma(x, y)$ the free-surface displacement; k $(= 2\pi / L)$ the wave number, L the wave length, and

$$P = \frac{\omega}{\lambda} , \qquad (2)$$

$$G = \frac{1}{2}\left(1 + \frac{2\lambda h}{\sinh 2\lambda h}\right) P , \qquad (3)$$

$$k^2 = \lambda^2 \left(1 - \frac{f^2}{\omega^2}\right) \qquad (4)$$

where $\omega\ (= 2\pi / T)$ the wave frequency with respect to wave period: T ; $f\ (= 2\,\Omega \sin\varphi)$ the Coriolis parameter, $\Omega\ (= 7.3\times10^{-5} S^{-1})$ the angular frequency of rotating earth, φ the latitude in degree; $h(x, y)$ the water depth; λ the intrinsic wave length satisfies with the characteristic equation:

$$\omega^2 = g\lambda \tanh\lambda h . \qquad (5)$$

Without losing the generality in solving Eq. (1), the

incident wave is expressed as:

$$\varsigma^I = A_0 e^{ik_0 r\cos(\theta-\theta^I)}, \tag{6}$$

where A_o and k_o are the amplitude and wave number of incident wave, respectively; θ^I the incident angle measured from positive x axis in counterclockwise sense. In the computational domain: Θ, in which the interested water area has been discretized with linear triangular isoparametric elements, the free surface displacement in the computational domain in general can be expressed by linear superposition as:

$$\varsigma = \varsigma^I + \varsigma^S, \tag{7}$$

where ς^S represents the scattered waves and satisfies the local radiation (non-reflective) condition on the open-sea artificial boundary: Γ_o:

$$\frac{\partial \varsigma^S}{\partial \vec{n}} - ik\varsigma^S = 0. \tag{8}$$

It is worth pointing out that Eq. (8) is used to overcome the numerical difficulties arise from specifying open boundary conditions which are usually unknown except at a very few field stations. Since the depths along the open boundaries do not always pertain to constant, local wave number k in Eq. (4) is thus implemented. Furthermore, Eq. (8) has been validated when the location of open boundary is at least one and half times of incident wavelength away from a scatter (Chen and Tsay, 1990). However, it regulates the scattered waves in outgoing directions. Along the irregular coastlines: Γ_{c_1} and Γ_{c_2}, the impermeable or zero-depth boundary condition:

$$PG\frac{\partial \varsigma}{\partial \vec{n}} = 0, \tag{9}$$

or

$$\frac{PGf}{f\sin(\theta_n-\phi)+i\omega\cos(\theta_n-\phi)}\frac{1}{r}\frac{\partial \varsigma}{\partial \phi} = 0, \tag{10}$$

is applied, where $\vec{n}$ denotes the outward normal unit vector of specific position located on the coastal boundaries; (r,ϕ) the corresponding polar coordinate; θ_n the normal angle on position (r,ϕ), and both of θ_n and ϕ are measured in counterclockwise direction, $i=\sqrt{-1}$ the imaginary number.

Applying the Galerkin finite elements method to Eq. (1) subjected to the boundary conditions: Eq. (8) and (10), the model equation then can be reformulated as:

$$\begin{aligned}&\iint_\Theta \left[\nabla W\cdot(PG\nabla\varsigma) - k^2 PGW\varsigma\right]dA + \oint_{\Gamma_{c1}} WPG\frac{D}{r}\frac{\partial\varsigma}{\partial\phi}\,dl \\ &-\oint_{\Gamma_o} WPG\left[ik\varsigma\cos(\theta_n-\phi)+\frac{1}{r}\frac{\partial\varsigma}{\partial\phi}\sin(\theta_n-\phi)\right]dl \\ &-\oint_{\Gamma_{c2}} WPG\frac{D}{r}\frac{\partial\varsigma}{\partial\phi}\,dl \\ &= \oint_{\Gamma_o} WPG\; i\cos(\theta_n-\phi)[k-k_o\cos(\phi-\theta^I)]\,\varsigma^I\,dl,\end{aligned} \tag{11}$$

where W is the shape function, and

$$D = \frac{f}{f\sin(\theta_n-\phi)+i\omega\cos(\theta_n-\phi)}. \tag{12}$$

Integrating and assembling all the elements by Eq. (11), a linear matrix equation is obtained (Tsay, et al., 1989; Chen and Tsay, 1990):

$$[\mathbf{M}]\{\varsigma\} = \{\mathbf{F}\}, \tag{13}$$

where $[\mathbf{M}]$ is an asymmetrical stiffness matrix due to the application of local boundary condition, and $\{\mathbf{F}\}$ the forcing matrix mainly induced by incident waves. Consequently, $\{\varsigma\}$ can be solved directly by using the Gaussian elimination method. It is noted that matrix $[\mathbf{M}]$ and $\{\mathbf{F}\}$ have complex constants, so is $\{\varsigma\}$ a complex vector too. The free surface displacement, therefore, can further be expressed in forms of amplitude and phase angle by using Euler's formula. The co-range with associated equi-phase charts then can be achieved in computational domain by calibrating the computed amplitudes and the phase angle with respect to a referenced station.

3. Computation results and verifications

The frequency-domain model is different from traditional time-domain model of which the Dirichlet conditions have to be pre-set on the open-sea boundary. To solve the spatial distributions of computed amplitudes as well as phase angles from Eq. (11), only the incident angle θ^I is needed to calibrate in computations. Choosing a computational domain located around Taiwan, numerical experiments for the best-fit results to the measurements are calibrated. It is found that the semidiurnal constituents with incident angle of 90° give the best results and are shown in this paper.

Spatial distributions of computed amplitudes and phase angles of $\mathbf{M_2}$, the predominant constituent in the Taiwan Strait (Lin, et al., 2000a), are shown in Figs. 1 and 2, respectively. Evidently, one can identify from Fig. 1 that there is a form of partially standing wave (Lin, et al., 200b) appearing in the Taiwan Strait. One node of the partially standing wave is located at the northeast coast between Su-Ao and Kee-Lung. The other node is located

at the southwest coast between An-Ping and Kao-Hsiung. From spatial gradient of equi-phase lines, Fig. 2, one can find that tidal waves encounter with each other at the northwest coast near Tao-yuang. Shape gradient of computed phase angles are noted near both of the nodes of the partially standing tides. Moreover, both spatial distributions of computed amplitudes and phase angles of $\mathbf{M_2}$ constituent appear almost symmetrically with respect to the central-west coast. The peculiar characteristics of tides, such as abnormal tidal range at the central-west coast, and significant variations of high-water time at both of the northeast and southwest coast, have been demonstrated accordingly by Lin et al., (2000b).

The computed results are calibrated according to the constituent harmonic constants of station Tai-Chung. The comparisons of amplitudes and phase-lags between field measurement data and computed results of $\mathbf{M_2}$ constituent around the coast of Taiwan are shown in Figs. 3 and 4, respectively. It is noted that both of the computed amplitudes and phase-lags show good agreements with the measurement ones. However, significant discrepancies in comparing the phase-lags are found respectively at the northeast coast from Yan-Liao to Kee-Lung and at the southwest coast from Kao-Hsiung to Xun-Guang-Zui, where near to the nodal locations of the partially standing wave.

For further reference, comparisons of amplitudes and phase-lags between field measurement data and computed results of $\mathbf{K_1}$ constituent around the coast of Taiwan are shown in Figs. 5 and 6, respectively. A general agreement is observed in the comparisons of computed amplitudes and the measured ones. In comparison of phase-lags, it is noted that the trend of distributions of phase-lags is not captured by present computations, even though the maximal discrepancies generally are no more than 45°. Furthermore, it is worth pointing out that the discrepancies between the computed phase-lags and the measured ones are extensively detected at locations near to the nodes of the partially standing wave. These discrepancies may be induced by the crude representation of local topography, or caused from the calibrated incident angle, which is set the same as that of semidiurnal constituent. Further computational improvements as well as corresponding investigations are currently under way.

4. Tidal prediction/hindcasting

Employing the tidal package (DHI, 1994) of IOS (the Institute of Ocean Sciences) with proper site-dependent harmonic constants (amplitude and phase-lag) of main tidal constituents, the prediction/hindcasting tidal elevation time series can be generated in demanded duration at specific site. To verify the hindcasting capability of the IOS package, the computed harmonic constants of the main tidal constituents: M_2, S_2, N_2, K_1, O_1, and P_1, of station Tai-Chung (TC) is predicted first. Special cares must be taken at the reference station TC, where the computed harmonic constants actually are the same as the ones of harmonic analysis. The prediction result (solid line in black) associated with the field data (solid line in red) during a month period of Nov., 1994, are shown in Fig. 7. Good agreements are observed by comparing the predicted results with the field data. This indicates that the tidal elevation time series can be regenerated by directly substituting the computed harmonic constants of the main tidal constituents: M_2, S_2, N_2, K_1, O_1, and P_1, of a specific site into the IOS package.

The predicted results at stations of Su-Ao (SA), Yan-Liao (YL), Kee-Lung (KL), Tan-Shui (TS), Hsin-Chu (HC), Pen-Hu (PH), Dong-Shi (TG), Kao-Hsiung (KH), Xun-Guang-Zui (SK), and Cheng-Kuang (CK) are shown in Fig. 8 (a) to (j), respectively. In the figures, the field data is denoted by solid line in red with annotation "Measured". For comparison reference, there are two predicted results demonstrated in Fig. 8. One is predicted by using the computed harmonic constants and is denoted by solid line in black with annotation "Computed". The other one is predicted by using the conventional harmonic analysis constants and is denoted by dash line in blue with annotation "IOS".

Comparing the "measured" data with "Computed" prediction at these stations, Fig. 8, the accuracies of tidal elevation of spring tide generally are better than that of neap tide. Deviations occur at stations near the nodes of the partially standing wave, Figs. 1 and 2. Disagreements generally are found in the phase shift. Most of the predicted tidal elevations are in good agreement with measured ones. The trend of tidal elevations in monthly duration generally is well captured by using the computed harmonic constants. Moreover, high precisions are observed at stations TS, HC, PH, and TG. General agreements are observed at stations SA, KH, SK, and CK. The worse cases are found at stations of YL and KL.

Geographically speaking, good agreements are observed at the sites along the west coast of Taiwan. Acceptable agreements are noted at the sites locating along the east coast. Discrepancies are found respectively at the sites around the northeast and southwest coasts, near to the nodes of the partially standing wave. From Figs. 3 to 6, it is noted that worse predictions mostly occur at the sites with large discrepancies in computed phase-lags, or with small amplitude of semidiurnal constituents. On the contrary, good prediction can always be found at the sites with relatively large amplitude of semidiurnal constituents. This shows that the diurnal constituents will affect tidal prediction, particularly in phase shift, in case of the semidiurnal constituents are not predominant.

5. Conclusion

Basing on the accuracy of tidal prediction, it is concluded that present approach to compute spatial distribution of tides provides a mean for tidal predictions at gauged and ungauged sites. Although the prediction accuracy still needed to be improved, present approach provides a method to gain the time series of tides at

arbitrary sites of interests. The accuracy of present approach can be improved when tides of diurnal constituents are obtained more accurately.

References

1 · Tsay, T. K., W. Zhu and P. L.-F. Liu (1989): A finite element model for wave refraction, diffraction, reflection and dissipation. J. Applied Ocean Res., 11, 33-38.

2 · Chen, B. S. and T. K. Tsay (1990): Application of local radiation condition to water-wave numerical modeling. Proc. 12th Conf. on Ocean Engrg., CICHE, 1-18 (in Chinese).

3 · Tsay, T. K. (1991): Linear surface waves over rotating fluids. J. waterway, Port, Coastal, and Ocean Eng., 117, 156-171

4 · DHI (1994): MIKE 21-Coastal hydraulics and oceanography tidal analysis and prediction module. User Guide, release 2.4, Danish Hydraulic Institute.

5 · Lin, M. C., W. J. Juang and T. K. Tsay (2000a): Anomalous amplification of semidiurnal tides along the western coast of Taiwan. Ocean Engineering, to appear.

6 · Lin, M. C., W. J. Juang and T. K. Tsay (2000b): Applications of the mild-slope equation to tidal computations in the Taiwan Strait. Journal of Oceanography, to appear.

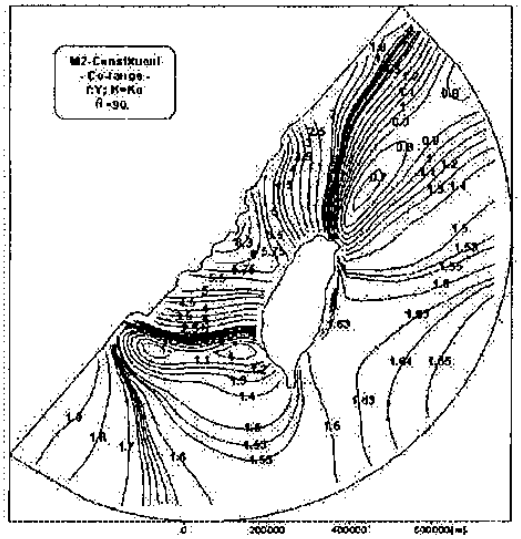

Fig. 1 Distribution of computed amplitudes of M_2 constituent around Taiwan.

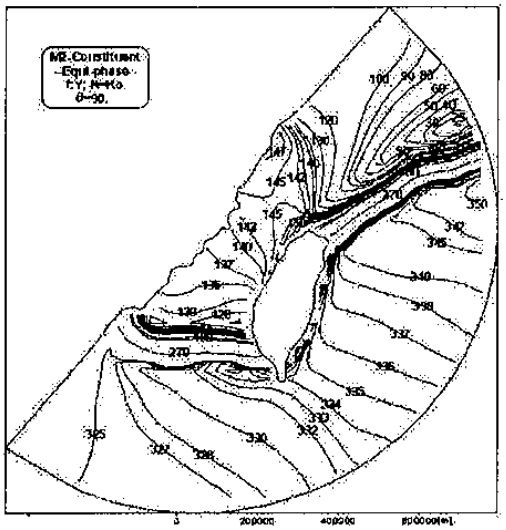

Fig. 2 Distribution of computed equi-phase lines of M_2 constituent around Taiwan.

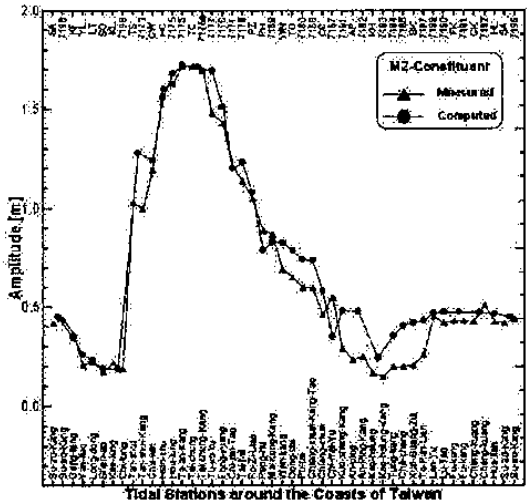

Fig. 3 Comparison of amplitude distribution of M_2 constituent around Taiwan.

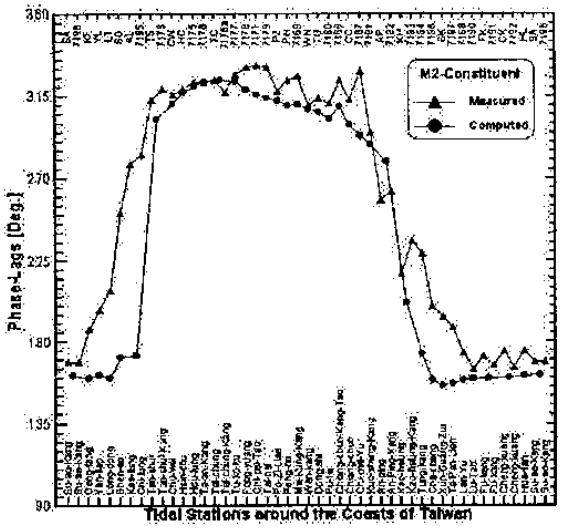

Fig. 4 Comparison of phase-lag distribution of M_2 constituent around Taiwan.

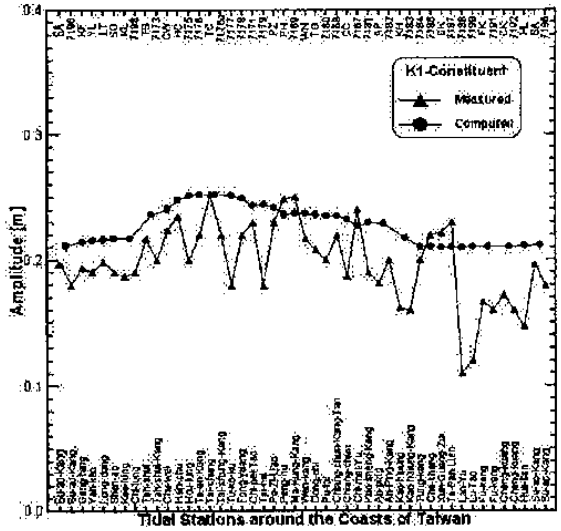

Fig. 5 Comparison of amplitude distribution of K_1 constituent around Taiwan.

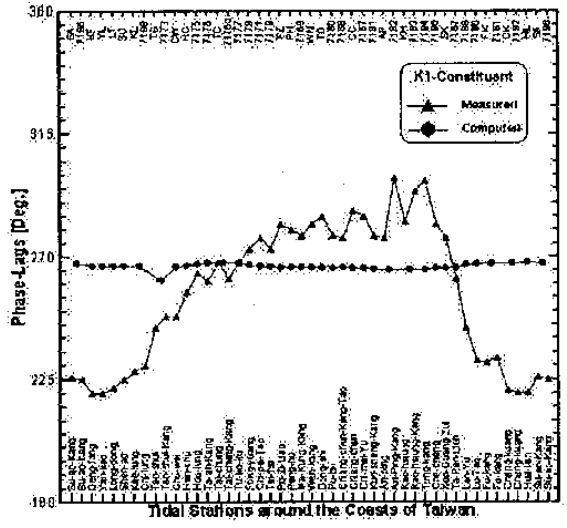

Fig. 6 Comparison of phase-lag distribution of K_1 constituent around Taiwan.

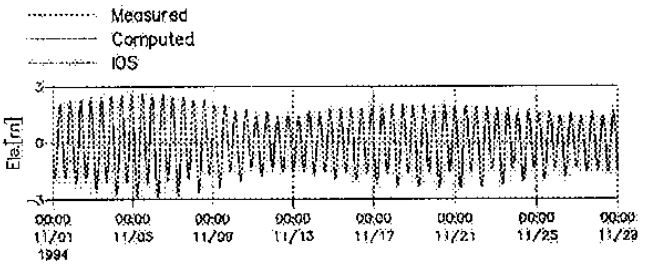

Fig. 7 Comparisons of tides at station TC.

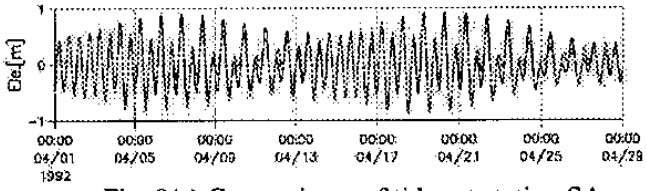

Fig. 8(a) Comparisons of tides at station SA.

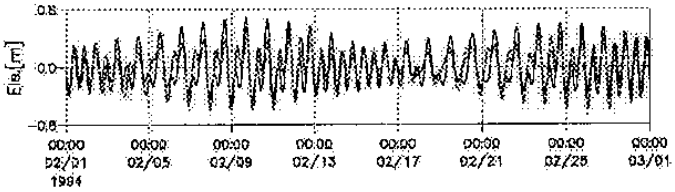

Fig. 8(b) at station YL.

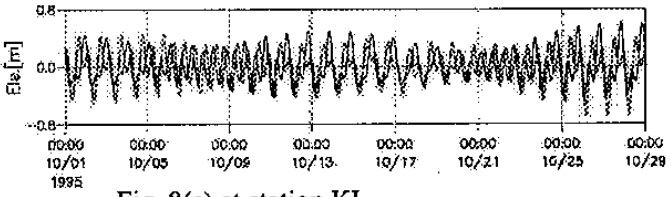

Fig. 8(c) at station KL.

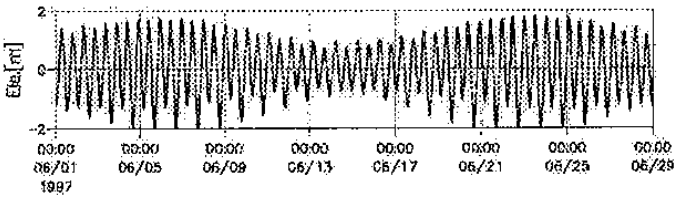

Fig. 8(d) at station TS.

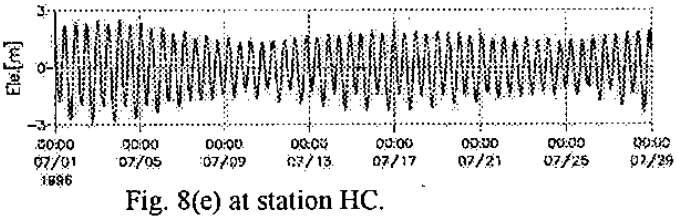

Fig. 8(e) at station HC.

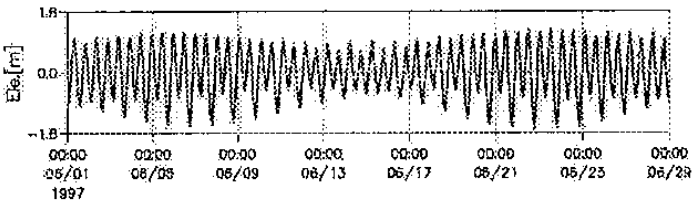

Fig. 8(f) at station PH.

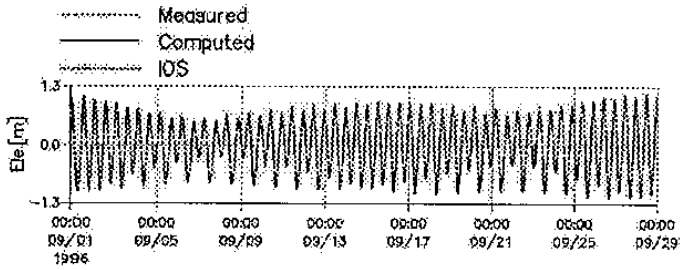

Fig. 8(g) Comparisons of tides at station TG.

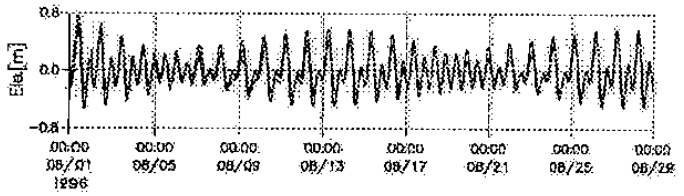

Fig. 8(h) at station KH.

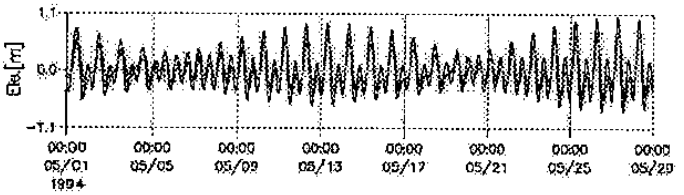

Fig. 8(i) at station SK.

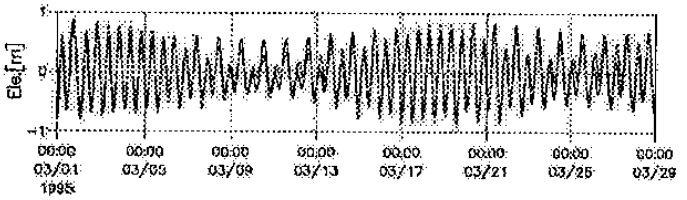

Fig. 8(j) at station CK.

頻率領域模式在潮汐預報上之應用

莊文傑[1]　蔡丁貴[2]　林銘崇[3]

[1]交通部運輸研究所港灣技術研究中心 研究員
[2]國立臺灣大學土木工程學系 教授
[3]國立臺灣大學造船暨海洋工程學系 教授

摘　要

本文使用含科氏力效應之二維線性淺水波模式以計算臺灣環島海岸潮汐主要分潮之調和常數，經 Lin, et al., (2000b) 驗證後，證實計算所得之調和常數準確性在半日潮時甚佳，故再進一步應用計算所得之調和常數，並結合 IOS 潮汐預報軟體以進行實際潮汐之預報。透過與實測資料之比較及驗證，由驗證結果可知，當大潮期間或驗潮站之潮汐明顯屬半日潮型，則應用本模式計算所得之調和常數進行實際潮汐預報之結果將與實測資料甚為符合。驗潮站之潮汐若屬混合偏全日潮型，則潮汐預報之結果與實測資料之吻合度稍差。普遍之預報誤差於小潮期間最明顯。儘管目前採用本計算所得之調和常數進行實際潮汐預報之準確度尚有待提昇，不過本文透過全面性調和常數之計算，可提供無驗潮站海域之潮汐逐時資料。